Atmos. Chem. Phys., 6, 2581–2591, 2006
www.atmos-chem-phys.net/6/2581/2006/

Atmospheric Chemistry and Physics

The quantitative infrared and NIR spectrum of CH_2I_2 vapor: vibrational assignments and potential for atmospheric monitoring

T. J. Johnson, T. Masiello, and S. W. Sharpe

Pacific Northwest National Laboratory, Richland, WA 99354, USA

Received: 15 November 2005 – Published in Atmos. Chem. Phys. Discuss.: 17 February 2006
Revised: 16 May 2006 – Accepted: 16 May 2006 – Published: 4 July 2006

Abstract. Diiodomethane (CH_2I_2) has recently become a molecule of significant atmospheric interest as it can contribute to coastal IO formation. As part of the PNNL database of gas-phase infrared spectra, the quantitative absorption spectrum of CH_2I_2 has been acquired at $0.1\,cm^{-1}$ resolution. Two strong b_2 symmetry A-type bands at 584 and $1114\,cm^{-1}$ are observed, but are not resolved when broadened to 760 Torr with nitrogen and appear as B-type. In contrast, the b_1 symmetry C-type bands near 5953, 4426 and $3073\,cm^{-1}$ are resolved with rotational structure, including Q-branches with widths $\leq 1\,cm^{-1}$. The quantitative infrared and near-infrared vapor-phase spectra (600–$10\,000\,cm^{-1}$) are reported for the first time. Some bands are discussed in terms of their potential for atmospheric monitoring and theoretical detection limits on a selected basis. FT-Raman spectra and ab initio calculations are used to complete vibrational assignments in the C_{2v} point group.

1 Introduction

Twenty-five years ago Chameides and Davis (1980) suggested the potential importance of iodine in tropospheric chemistry. They recognized that certain species such as methyl iodide, CH_3I, are easily photolyzed to liberate atomic iodine, which can react with O_3 and then NO_x or HO_x to form other inorganic species such as IO, HOI or $IONO_2$. The analogous reactions for diiodomethane, CH_2I_2, are:

$$CH_2I_2 + h\nu \rightarrow CH_2I + I \quad (1)$$

$$I + O_3 \rightarrow IO + O_2 \quad (2)$$

$$IO + HO_2 \rightarrow HOI + O_2 \quad (3)$$

$$IO + NO_2 \rightarrow IONO_2 \quad (4)$$

Correspondence to: T. J. Johnson
(timothy.johnson@pnl.gov)

Similar to the ClO_x and BrO_x systems, the various iodine species can be cycled back to a radical I atom with catalytic O_3 destruction and an increase in the NO_2/NO ratio. Subsequent works continue to emphasize the importance of iodine in atmospheric chemistry (Solomon et al., 1994). Although typical concentrations are low (sub-ppb_v), most organic iodides are readily photolyzed in the visible and near-UV and the ensuing kinetics are typically fast, thus leading to the importance of the iodine cycles.

In addition to CH_3I, the photolysis of CH_2I_2 was also investigated some years ago where it was suggested that I_2 can appear as an end photoproduct and at high concentrations there is regeneration of the parent compound (Schmitt and Comes, 1980; Kasper et al., 1964, 1965). More recently and more importantly, the photolysis of CH_2I_2 has had renewed interest since laboratory experiments have shown that the photolysis of certain iodine-containing species in the presence of ozone (O_3) plays a direct role in the formation of aerosols (Jimenez et al., 2003; Kolb, 2002; Burkholder et al., 2004). It has been shown that the photolysis of CH_2I_2 in the presence of ozone results (via Reaction 2) in IO, and CH_2I_2 is thus a major contributor to coastal IO formation. Field experiments have subsequently shown that the seas are a direct source of several gas-phase halogenated species, (McFiggans et al., 2004; Carpenter et al., 1999) including CH_2I_2. Diiodomethane and other alkyl iodides have been identified with maritime biogenic sources, (Carpenter et al., 1999) in particular *Laminaria* Macroalgae (McFiggans et al., 2004) or the brown algae *Fucus* (Mäkelä et al., 2002). The existence of the iodine dioxide molecule, OIO, was first observed in the laboratory by Himmelmann et al. (1996). Ravishankara and co-workers (Harwood et al., 1997; Gilles et al., 1997) first investigated the kinetics of the IO radical reacting either with BrO or with itself, while Cox and colleagues (Bloss et al., 2001; Rowley et al., 2001; Cox et al., 1999) first observed OIO as a primary reaction product:

Published by Copernicus GmbH on behalf of the European Geosciences Union.

$$IO + XO \rightarrow OIO + X \qquad X=Br, I. \tag{5}$$

Tucceri et al. (2006) have recently measured the OIO absorption cross-sections using pulsed laser photolysis. O'Dowd and co-workers have also shown that nucleation was observed over several orders of magnitude in CH_2I_2 and suggested that the gas-phase OIO is responsible for the new particle growth (Jimenez et al., 2003; Mäkelä et al., 2002). CH_2I_2 photolysis in the presence of ozone thus plays a role in marine boundary layer ozone loss (Vogt et al., 1999).

In terms of spectroscopy, relatively little has been reported regarding gas-phase CH_2I_2. The early photolysis work of Pimentel and co-workers, as well as Kroger et al. (1976) and Schmitt and Comes (1980) showed that photolysis liberates an I atom and an internally excited CH_2I radical. Vibrational spectra of CH_2I_2 liquid have been reported previously by both Ford (1975) and Voelz et al. (1953), with the fundamentals being assigned in the C_{2v} point group, as well as a few combination and overtone bands. Although both the liquid- and vapor-phase spectra have been recorded in the IR, (Ford, 1975; Voelz et al., 1953), it appears the resolution was not sufficient to resolve any ro-vibronic structure in the vapor. There have also been assignments made of the $\Delta\nu_{CH}$=3, 4, 5 and 6 overtones in the near-infrared spectrum, (Henry and Hung, 1978) but these were also in the liquid phase. The anharmonicity was used to extrapolate a fundamental frequency of 3059 cm^{-1} for the liquid, which would correspond to the C-H stretch ν_6 fundamental (vide infra). While Marshall et al. (2005) have calculated frequencies, but not intensities, of CH_2I_2 using ab initio methods, to date there have been no quantitative vapor spectra of this moderately volatile species (1.2 Torr at 298 K).

The Pacific Northwest National Laboratory (PNNL) continues to construct a reference library of quantitative high-resolution infrared spectra designed for tropospheric monitoring (Sharpe et al., 2004). This Northwest Infrared (NWIR) database, is optimized for best signal-to-noise ratio (SNR) in the long-wave infrared (LWIR), 800–1300 cm^{-1}, but each spectrum has a minimal spectral range of $\leq$600 to $\geq$6500 cm^{-1}. When certain bands are recognized as having sufficient SNR outside this minimal spectral range, these data are also included. The reference spectra are intended primarily for open path monitoring; each laboratory measurement has the analyte back-pressurized with ultra-high purity (UHP) nitrogen to 760$\pm$5 Torr. The data are nevertheless recorded at 0.112 cm^{-1} resolution in the desire to bring out all possible spectral features, not only the resolved ro-vibronic lines of lighter species, but also the Q-branches of many polyatomics that display halfwidths of 1 cm^{-1} or less. Recognizing that most species have typical pressure broadening coefficients of $\sim$0.1 cm^{-1}/atm, additional resolution was deemed unnecessary for these reference data.

While constructing the NWIR database, it was recognized that CH_2I_2 has recently garnered great interest among the atmospheric community, and it would be beneficial to point out alternate method for monitoring this trace gas. While GC/MS offers excellent sensitivity for CH_2I_2 analysis, it is limited to point measurements (Wevill and Carpenter, 2004). Since estimated maritime boundary layer concentrations are at most 100's of ppt_v, it was recognized that the only optical methods with sufficient sensitivity to see CH_2I_2 would be, for example, long path DOAS (Platt, 1994) or narrow-band IR laser techniques (Johnson et al., 1991a; Sharpe et al., 1998): Special attention was thus paid to narrow spectral features: e.g., transitions over which a probing laser frequency can easily be tuned.

2 Experimental

Using the methods of Chu et al. (1999) and Sharpe et al. (2004) a series of measurements is made, each corresponding to a different concentration-path length burden. Each fitted spectrum, in fact, represents a series of (typically $>$10) individual measurements at 298.1 K, with the different measurements covering a large range (often $>$2 orders of magnitude) of analyte burdens, each burden pressurized with UHP N_2 to one atmosphere. The fitted spectrum is derived by fitting a Beer's law plot at each wavelength channel to each of the individual burdens. In order to account for any of several different nonlinearity phenomena in the A=f(P) fit, the individual burdens are in addition weighted according to T^2 (where $T=I/I_o$). All values with $T<0.025$ (i.e. decadic absorbance $A>1.6$) are weighted with zero. This multiple burden with weighted data approach retains several advantages over any single measurement or few measurements: First, multiple measurements greatly enhance the SNR ratio. Second, the high burden measurements enhance the SNR for the weak bands that might not exceed the noise floor in any measurement designed to keep the strong bands on scale. Third, for the strong bands, the weighting mechanism brings out a better fidelity to account for Beer's law saturation effects, photoconductive detector nonlinearity effects or other phenomena that cause the absorbance values to not scale with burden. Finally, analyzing the residual vector has proven helpful at recognizing chemical impurities as their signatures typically do not scale with the fit.

Allen et al. (2005) have also recently published the advantages of fitting the absorbance as a function of partial pressure in order to calculate $A(\lambda)$, as first discussed by Chu et al. (1999). The Chu et al. methods go further, however, that in addition to the absorbance data linear fit at each wavelength bin, the raw data also have a weighting factor to account for nonlinearity mechanisms. In this method the residual fit vector is, moreover, carefully analyzed since any chemical impurities, including the uncommon ones, readily manifest themselves in the residual. The PNNL method typically measures twelve to fifteen separate burdens ranging over two orders of magnitude. The resulting error analysis (Sharpe et al., 2003) shows that the maximal expected

systematic errors in absorbance are 3% for the PNNL static system measurements and 7% for flow system measurements, including the CH_2I_2 values reported here. The measured random values are less than this, and these results have been vetted against NIST for a host of different molecules as described by Sharpe (2003, 2004), which contain further details of the error analysis. The above discussion is valid for each of the 400+ molecules in the PNNL database. In addition, for CH_2I_2 and a handful of other species, high resolution ($0.0015\,cm^{-1}$) studies have assigned all observed bands to the analyte, increasing confidence as to chemical purity. (Maki et al., 2001; Masiello et al., 2005).

The CH_2I_2 sample itself was from Aldrich Chemicals and its purity was monitored by comparing to known infrared spectra. A Bruker IFS 66v/S vacuum spectrometer (Johnson et al., 2005) was used over the 600 to $6500\,cm^{-1}$ range. The spectrometer hardware characteristics have been previously documented (Johnson et al., 2002) according to IUPAC guidelines, (Bertie et al., 1998) taking care to avoid ghosting, "warm aperture" (Johnson et al., 2002) and detector nonlinearity (Chase, 1984; Birk et al., 1996) artifacts. Due to the modest vapor pressure of CH_2I_2 (1.2 Torr at 298 K, Yaws, 1999) these measurements were made on a long path flowed system whereby the liquid analyte is quantitatively delivered into a heated stream of ultra-high purity N_2 carrier gas, (Sharpe et al., 2003) using a specially constructed vapor dissemination system (Johnson et al., 2006[1]). The measurement at 298.1 K is made in a specially designed White cell with a circulating liquid jacket which can provide more precise temperature control (Ballard et al., 1994) with the optical path set to 7.96 m (±0.5%). The temperature is measured by placing a NIST-traceable temperature probe directly into the gas in the White cell; the stated accuracy is ±0.2 K. For each of the 12 burdens, 256 interferograms were averaged to reduce noise. Gain ranging improved the signal-to-noise by amplifying the wings of the interferogram before digitization. The single-sided interferograms were zerofilled 2× and phase corrected using Mertz's method (Mertz, 1967). Decadic absorbance spectra were calculated in the usual manner $[-\log(I/I_o)]$ using the spectrum of the cell with just N_2 carrier gas for I_o. The final data product is a spectrum that corresponds to an optical path of 1 m through a mixing ratio of 1 ppm_v of analyte at 296 K.

For this particular molecule, several bands of interest were noted in the near-infrared (NIR) range, so seventeen additional burdens were measured with alternate hardware optimized to improve the NIR signal/noise. These included a tungsten halide source, a Si/CaF_2 beamsplitter, and a photovoltaic InSb detector. The mirror scan speed was adjusted to 20 kHz, but all other collection parameters were as for the mid-infrared measurements (Sharpe et al., 2004). The NIR spectra covered the 1900 to $10\,000\,cm^{-1}$ range, for a total range of 550–$10\,000\,cm^{-1}$. Data are only plotted to $6500\,cm^{-1}$ as the few bands at higher frequencies are relatively weak. The FT-Raman spectra were collected over the range from 50 to $3600\,cm^{-1}$ Stokes shift and from -100 to $-1000\,cm^{-1}$ anti-Stokes shift using a previously described instrument (Williams et al., 2006). Raman frequencies are calibrated using the interferometer HeNe laser and the Raman Nd:YAG laser. For a given FT-Raman spectrum the frequency accuracy has been shown to be better than $1\,cm^{-1}$. Data collection parameters and methods for the low pressure, high resolution IR spectra ($0.0015\,cm^{-1}$ on a Bruker IFS 125), including for peaks reported in the far-IR, have already been reported by Maki et al. (2001). Theoretical ab initio calculations were performed using the NWChem software algorithm. The vibrational frequencies and infrared line intensities (peak maxima) were calculated at the MP2 level with the largest basis set (6–311 g**) possible that delivers both frequencies and intensities; the frequencies are typically too large, and are customarily scaled by a factor of 0.955 (Marshall et al., 2005).

3 Results

Figure 1 reports the quantitative gas-phase infrared spectrum[2] of methylene iodide (diiodomethane) from 550 to $6500\,cm^{-1}$. The y-axis is quantitative such that the absorbance values correspond to an optical path of 1 m through a concentration of 1 ppm_v of analyte at 296 K and 1 atm total pressure. The reported spectrum represents the weighted average of 12 individual measurements for the mid-infrared and 17 measurements for the near-infrared. The concatenated spectrum has been broken into four separate plots for visual clarity. Note that the plot in Fig. 1a has a different ordinate scale as the ν_9 band at $584.21\,cm^{-1}$ and the ν_8 band at $1113.87\,cm^{-1}$ are both IR-allowed fundamentals and are very intense bands. Plots 1b, 1c and 1d are all on the same scale, and all plots represent an average from multiple burdens of CH_2I_2, each burden pressure-broadened to 760 Torr. The peak positions and band types of the fundamentals for the present vapor-phase data are given in Table 1. Also in Table 1 are the corresponding liquid-phase values, both infrared and Raman, as well as the vibrational assignments. Table 2 presents the integrated vapor-phase band strengths (in units of $cm^{-1}\,cm^2\,molecule^{-1}$, or $cm\,molecule^{-1}$) for the fundamentals. While the data in the NWIR database use base 10 logarithms, the band integrals in Table 2 use Naperian (natural) logarithms at 296 K for the peak height as this is the more common unit for S. Also in Table 2 are the frequencies and intensities as calculated by the ab initio program NWChem. As these are the first Fourier-transform measurements of vapor-phase CH_2I_2 the accuracy along the

[1] Johnson, T. J., Sharpe, S. W., and Covert, M. A.: A Method for Quantitative Dissemination of Vapors, Review of Scientific Instruments, in review, 2006.

[2] The CH_2I_2 spectrum and other NWIR data can be found at http://nwir.pnl.gov.

Table 1. Observed Raman (liquid), Infrared (liquid and gas) vibrational frequencies, Raman polarizations and (for vapor measurements) band types of CH_2I_2, together with symmetries and vibrational assignments. Frequencies are in cm^{-1}. Fundamental frequencies are printed in bold. Details can be found in text. NS = not seen, OOR = out of range.

Ram Liq	Ram str	Ram Polz	IR Liq	Liq Str	IR Gas	Band Type Rel. Intens.	Assm't	SYM
121	**vs**	**pol**	**122**	**w**	**NS**		$\boldsymbol{\nu_4}$	$\mathbf{a_1}$
197	w	pol	NS	NS	NS			
238	w	pol	NS	NS	NS		$2\nu_4$	A_1
365	w	pol	NS	NS	NS		$\nu_3-\nu_4$	A_1
448	vw		448		463.79		$\nu_9-\nu_4$	
486	**vs**	**pol**	**485**	**w**	**493.01**	**B–vw**	$\boldsymbol{\nu_3}$	$\mathbf{a_1}$
571	**m**	**dp**	**571**	**s**	**584.21**	**A–vs**	$\boldsymbol{\nu_9}$	$\mathbf{b_2}$
604	w	pol	NS	NS			$\nu_3+\nu_4$	A_1
717	**w**	**dp**	**717**	**s**	**718.08**	**C**	$\boldsymbol{\nu_7}$	$\mathbf{b_1}$
851	w		851	vw	NS			
969	w	pol	NS	NS	NS		$2\nu_3$	A_1
1032	**w**	**dp**	**1033**	**w**	**1041.99**	**vw**	$\boldsymbol{\nu_5}$	$\mathbf{a_2}$
					1075.04	vw	$\nu_3+\nu_9$	B_2
1109	**m**	**dp**	**1106**	**vs**	**1113.87**	**A–vs**	$\boldsymbol{\nu_8}$	$\mathbf{b_2}$
1134	m	pol	NS	NS	NS	NS	$2\nu_9$	A_1
1181	vw		1181	w	1189.1	w	$\nu_3+\nu_7$	B_1
NS			1226	m	1229.42	A–s	$\nu_4+\nu_8$	B_2
1353	**m**	**pol**	**1352**	**m**	**1373.61**	**B–w**	$\boldsymbol{\nu_2}$	$\mathbf{a_1}$
1434	m	pol	NS	NS	NS		$2\nu_7$	A_1
			1595	vw	1603.39	w	$\nu_3+\nu_8$	B_2
1672	w	pol	NS	NS			$\nu_8+\nu_9$	A_1
			NS	NS	1714.86	C–w	$\nu_4+\nu_5+\nu_9$	B_1
1755	w	dp	1754	vw	1759.38	A	$\nu_5+\nu_7$	B_2
NS			1837		1864.97	w	$\nu_7+2\nu_9$	B_1
NS			1921	w	1953.86	w	$\nu_2+\nu_9$	B_2
1995	vw	pol	NS		NS			
2058	w	dp	2056		2075.67	C	$\nu_2+\nu_7$	B_1
NS			2132		2142.42	C–s	$\nu_5+\nu_8$	B_1
2209	w	pol	2209		2222.42	B	$2\nu_8$	A_1
2238	w	pol	NS	NS	NS			A_1
2360	w	pol	NS	NS	NS			A_1
2453	w	dp	2454		2482.14	A	$\nu_2+\nu_8$	B_2
2504	vw		NS		NS		$\nu_2+2\nu_9$	A_1
NS		NS	2549	vvw	2560.12	w	$\nu_2+\nu_3+\nu_7$	B_1
2602	m	pol	NS	NS	2631.70	vw	$2\nu_5+\nu_9$	B_2
2967	**vs**	**pol**	**2968**	**s**	**3002.00**	**B–s**	$\boldsymbol{\nu_1}$	$\mathbf{a_1}$
3046	**s**	**dp**	**3046**	**vs**	**3073.01**	**C–s**	$\boldsymbol{\nu_6}$	$\mathbf{b_1}$
3332	w	pol	NS	NS	3323.23	B–w		
3573	w	pol	NS	NS	3585.93	B–w	$\nu_1+\nu_9$	B_2
OOR			3757	m	3785.26	B–w	$\nu_6+\nu_7$	A_1
OOR			4061	m	4097.60	A/B–s	$\nu_5+\nu_6$	B_2
OOR			4377	m	4426.52	C–s	$\nu_2+\nu_6$	B_1
OOR			5852	w	5921.62	B–m	$2\nu_1$	A_1
OOR			5892	w	5953.31	C–m	$\nu_1+\nu_6$	B_1
OOR			6094	w	6102.68	B–m	$2\nu_6$	A_1

wavelength axis is much higher (Sharpe et al., 2004; Maki and Wells, 1991). High resolution vapor-phase infrared spectra confirm our low resolution estimates for many of the band origins given in Table 1. However, precise determination of the band origins can only be achieved through analysis of the high resolution data. Consequently, an error of $\pm 0.1\,cm^{-1}$

should be assumed for all values given in Table 1 for the vapor-phase spectra.

The vibrational assignments largely agree with those of Voelz and co-workers (1953) as well as Ford (1975). The nine fundamentals in the C_{2v} point group are printed in bold in Table 1. The long path gas cell and greater instrumental sensitivity allow for observation of even very weak fundamentals including ν_3 (a_1 symmetry, 493.01 cm^{-1}) ν_7 (b_1, 718.08 cm^{-1}) and ν_2 (a_1, 1373.61 cm^{-1}). The Raman spectra aided in the assignment and confirmation of many vibrational bands, especially the polarized Raman spectra which helped to confirm assignment of vibrational modes with a_1 symmetry. The symmetric ν_1 (3002.00), ν_2 (1373.61), ν_3 (493.01) and ν_4 (122 cm^{-1}) a_1 modes are easily assigned due to their medium to very strong Raman signals which are all strongly polarized (i.e. a_1 modes). We note that the ν_4 (122 cm^{-1}) fundamental was not observed in any of the IR gas-phase spectra, including path lengths >35 m. This diminished intensity does agree with that predicted by the ab initio calculations (Table 2). The ν_8 (1113.87) and ν_9 (584.21) IR bands are both b_2 modes and dominate the IR spectrum. Although both appear to be B-type bands in the pressure-broadened 0.1 cm^{-1} gas-phase measurements, high resolution (0.0015 cm^{-1}) measurements at low pressure do show A-type contours, and centralized Q-branch features as expected.

The ν_5 (a_2) fundamental is seen in both the liquid Raman and liquid IR spectra at 1033 cm^{-1}. As an a_2 mode, it is IR forbidden in the C_{2v} point group, but we can tentatively assign the very weak 1041.99 cm^{-1} band as the corresponding gas phase fundamental which has modest intensity in the liquid due to condensed phase interactions. The depolarized Raman signal helps assign the symmetry. The $\nu_3+\nu_9$ combination band is seen only in the gas phase at 1075.04 cm^{-1}, while the band at 2075.67 is the $\nu_2+\nu_7$ combination. Many of the overtone, combination and difference bands are assigned for the first time. In particular, we assign for the first time many of the bands at frequencies >3500 cm^{-1}. Although these frequencies are outside the Raman spectrum, the vapor-phase band profiles (Fig. 2), along with the NWChem ab initio calculations make the assignments straightforward in most cases.

In terms of band strengths, the b_2 ν_9 (584.21 cm^{-1}) and ν_8 (1113.87 cm^{-1}) bands are clearly the most intense IR bands and dominate the spectrum. Both are pressure broadened at 760 Torr (Nitrogen) to form unresolved bands that are B-type in appearance, but in fact are A-type. Of the two, ν_8 is the more intense with a width (FWHM) of 11.8 cm^{-1} and a peak amplitude 1.2×10^{-3} absorbance for 1 ppm-m. The spacing of the CH_2I_2 rotational lines in the ν_8 and ν_9 bands is quite small and these do not resolve at atmospheric pressure. They do resolve at low pressure, however, and a high resolution study assigning both these bands is currently under way in our laboratory using previously described high resolution instrumentation (Maki et al., 2001).

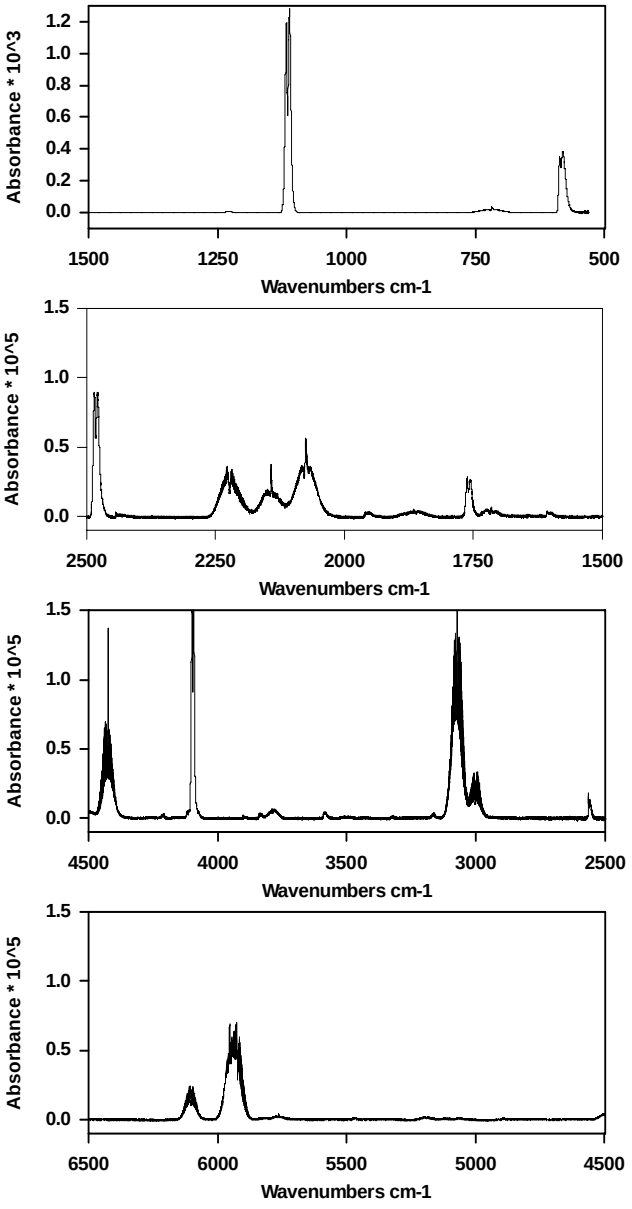

Fig. 1. Mid- and near-infrared quantitative spectrum of diiodomethane (CH_2I_2) from 6500 to 550 cm^{-1}, recorded at 0.1 cm^{-1} resolution. The spectrum is actually a composite derived from multiple spectra that corresponds to 1 ppm-m of gas at 296 K pressure-broadened to 760 Torr. Note that due to the strong bands at 584 and 1114 cm^{-1} panel **(a)** has been multiplied by 10^3, while panels **(b–d)** have been multiplied by 10^5 on the y-axis. See text for details.

For the remaining pressure-broadened bands shown in Fig. 1, many are of approximately the same band strength, and of these several are C-type bands that exhibit resolved Q-branches. We focus on these in particular, since the resolved structure better lends itself to open path monitoring, either via methods such as DOAS (Platt, 1994; Volkamer et al., 2005) or laser-based techniques. Three of these

Table 2. Observed Raman (liquid) and infrared (liquid and gas) vibrational frequencies along with gas-phase band integrals for the fundamental vibrations of CH_2I_2. Frequencies are in cm^{-1} and band integrals are in units of cm-molecule^{-1}, using Naperian (natural) logarithms at 296 K for the peak heights, and have been multiplied by 10^{18}. Also listed are the frequencies (scaled by 0.955) and IR intensities relative to ν_8 as predicted by NWChem. Details in text.

Assm't	SYM	Ram Liq	IR Liq	IR Gas	Gas Bnd $\int$ limits	Band $\int$ cm/molec	NWC Freq'y	NWC Ints'y
						296 K×1e18	Adjusted	Rel to ν_8
ν_4	a_1	121	122	NS	NS	NS	117	0.02
ν_3	a_1	486	485	493.01	NC	NC	476	0.15
ν_9	b_2	571	571	584.21	600–550	5.1240	579	28.60
ν_7	b_1	717	717	718.08	775–665	0.8785	705	9.02
ν_5	a_2	1032	1033	1041.99	1048–1031	0.0008	1045	–
ν_8	b_2	1109	1106	1113.87	1135–1090	13.0800	1135	100.00
ν_2	a_1	1353	1352	1373.61	1420–1330	0.0159	1366	0.16
ν_1	a_1	2967	2968	3002.00	3030–2950	0.0756	3030	0.26
ν_6	b_1	3046	3046	3073.01	3140–3030	0.4147	3111	2.80

bands with the C-type profile will be considered in more detail for pressure-broadened (ambient) monitoring. Figure 2's top trace displays the ν_1 fundamental at 3002.00 cm^{-1} along with the C-type ν_6 band at 3073.01 cm^{-1}, where the plot again represents an optical depth of 1 ppm-m. For the ν_6 band the Q-branch has a peak height of 2.65×10^{-5} OD with a Q-branch differential peak height of 1.98×10^{-5}. The middle trace of Fig. 2 plots the $\nu_2+\nu_6$ combination band at 4426.52 cm^{-1}, and the lower trace shows the $2\,\nu_1$ overtone at 5921.62 cm^{-1} along with the ($\nu_1+\nu_6$) combination C-type band at 5953.31 cm^{-1}. Note that the y-axis has been held the same in the three plots to show the relative line strengths, most of which are comparable, though all these bands are approximately two orders of magnitude weaker than ν_8 or ν_9 bands in the long-wave infrared.

4 Discussion

Both the intense IR fundamentals, ν_9 at 584.21 cm^{-1} and ν_8 at 1113.87 cm^{-1}, shown in Fig. 1 are in fact unresolved A-type bands and fall in an "atmospheric window". For low resolution monitoring, the ν_8 band at 1113.87 cm^{-1} is the most promising as it lies in the center of the LWIR window. We note that both the ν_8 and ν_9 fundamentals are of b_2 symmetry in the C_{2v} point group. At 0.1 cm^{-1} resolution and pressure broadened by N_2, both appear as B-type bands, but very high resolution spectra recorded at low pressure have shown the expected A-type structure. The ν_8 band has a width (FWHM) of 11.8 cm^{-1}, and a peak amplitude of 1.2×10^{-3} OD for 1 ppm-m. At lower resolution, typically 4 or 8 cm^{-1}, used in most ambient monitoring situations with an active or semi-active FTIR system (Johnson et al., 2004), the one minute detection limits are of the order 10^{-4} OD (Griffith and Jamie, 2000). This suggests that for a 500 m (open) path, an optimistic detection limit for CH_2I_2 is 500 ppt_v. Consequently, current FT-methods would be challenged to observe the anticipated <100 ppt_v biogenic levels of CH_2I_2 (Carpenter et al., 1999). Although they are the strongest bands, the ν_8 and ν_9 bands are unresolved at 760 Torr and may not be useful for open-path laser monitoring. As mentioned above, however, these bands do resolve at low pressure, and their assignments and potential for monitoring will be discussed in a separate work. We are optimistic that the line strengths are sufficient to be useful for extractive monitoring, using e.g. Pb-salt or QC-laser systems.

Of the laser methods, Pb-salt systems have been widely used in the mid-IR (λ=3 to 20 μm), primarily as point sensors using long path cells at low pressure (Werle et al., 2004). Several near-IR laser systems have been deployed using techniques such as FM modulation (Johnson et al., 1991b) or cavity ring-down methods (Bitter et al., 2005). Until recently, the greatest limitations appear to be the tunability and wavelength availability of the lasers, predominantly limited to the wavelengths used by the telecommunications industry

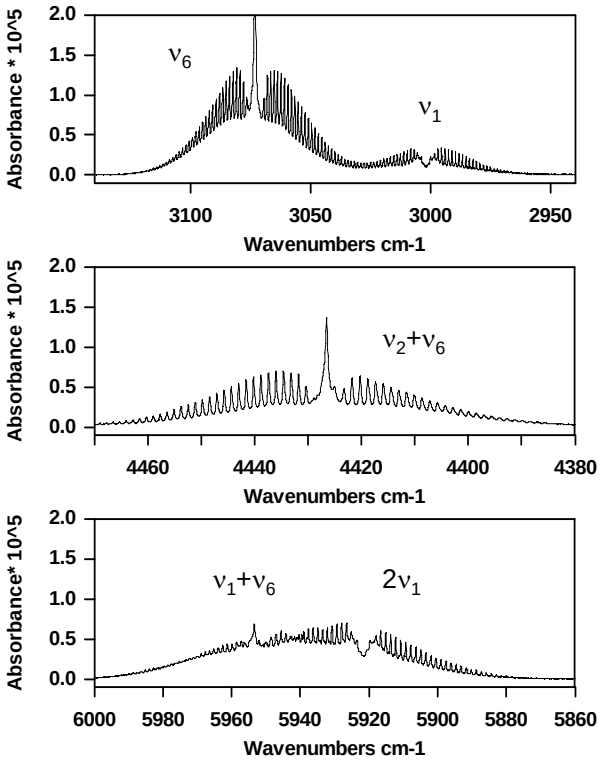

Fig. 2. Details of three spectral regions of interest for monitoring. The spectra are all pressure broadened to 760 Torr and are composite spectra that correspond to 1 ppm-m optical depth. The y-axis is on the same scale in all three panels. Panel **(a)** shows the ν_1 band (3002 cm^{-1}) along with the ν_6 band (3073 cm^{-1}), panel **(b)** shows the ($\nu_2+\nu_6$) combination band at 4427 cm^{-1}, while panel **(c)** shows the 2 ν_1 overtone band (5921 cm^{-1}) along with the ($\nu_1+\nu_6$) combination band at 5953 cm^{-1}.

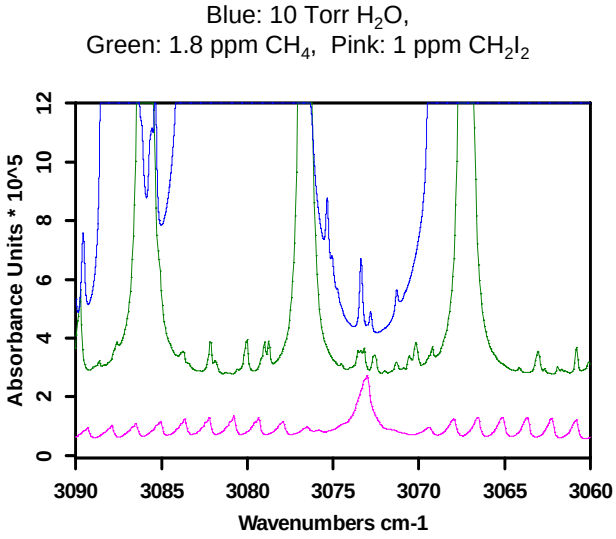

Fig. 3. Comparison plot (all at 0.1 cm^{-1} resolution) showing potential interferents to the CH_2I_2 ν_6 band at 3073.01 cm^{-1}. The traces correspond to 1 ppm-m of CH_2I_2 (lower trace – pink), 1.8 ppm-m of CH_4 (middle trace – green), and 10 Torr of H_2O (upper trace – blue). The H_2O data are from the HITRAN data base. The spectra have been vertically offset for clarity. See text for details.

(e.g. 1.3 or 1.55 μm). The recent advent of quantum cascade (QC) lasers shows excellent promise as these are available from the near-IR to the terahertz (THz) wavelengths. These lasers have also demonstrated an important feature in that they have significant tuning ranges, typically >0.5% or more of the central wavelength, depending on the nature of the device fabrication. This allows, for example, tuning across a 1 cm^{-1} wide Q-branch for atmospheric monitoring purposes.

Figure 3 demonstrates one possibility for monitoring using the Q-branch of the 760 Torr ν_6 band at 3073.01 cm^{-1}; this CH_2I_2 spectrum (1 ppm-m) is plotted in pink. Although 1 ppm is far greater than expected ambient concentrations, this may simulate a chamber experiment. Also plotted in Fig. 3 are 1 m paths for typical ambient concentrations (Warneck, 1988) of 1.8 ppm for methane (green) and the optical density corresponding to 10 Torr of H_2O (blue). The water data are from the HITRAN database (Rothman et al., 2005) since the HITRAN calculated data have no noise that can obfuscate the signal when expanded thousands of times. The database was examined for other potential interferents with high background concentrations (e.g. N_2O, CO_2, CO), but these did not show any interfering absorptions at these wavelengths. The Q-branch at 3073 cm^{-1} corresponds to a differential peak height of 1.98×10^{-5} OD for 1 ppm-m, which is also equivalent to 1.98×10^{-5} for 1 ppb-km. The 3.25 μm wavelength can be accessed by both Pb-salt and quantum cascade diode lasers. Assuming an open path laser-based system with a 10 km path length, in order to achieve a 50 ppt_v detection limit, a spectrometer would need a detection sensitivity corresponding to $\sim1\times10^{-5}$ OD or better. For an extractive laser-based system with a 200 m path length, in order to achieve a 50 ppt_v detection limit, a spectrometer would need a detection sensitivity corresponding to $\sim2\times10^{-7}$ OD or better at these wavelengths Although such a measurement would pose a challenge, the best extractive measurements at these wavelengths are now achieving such detection limits using difference frequency generation (Richter et al., 2002) or improved Pb-salt diode laser systems (Wert et al., 2003; Schiller et al., 2001). The weak methane lines near 3073 cm^{-1} pose a concern, but the CH_4 mixing ratios can be expected to be low and constant in marine atmospheres. It is also possible that using an extractive system with a near-infrared detector (e.g. InSb) and a long path cell that some of the lines in the Q-branch resolve and separate from those of methane, also possibly increasing the depth of any one of the CH_2I_2 lines. Orphal and Ibrahim (2005) have announced recent results showing that the ν_1 and ν_6 bands near 3.3 μm do resolve at low pressure and thus may be useful for extractive monitoring.

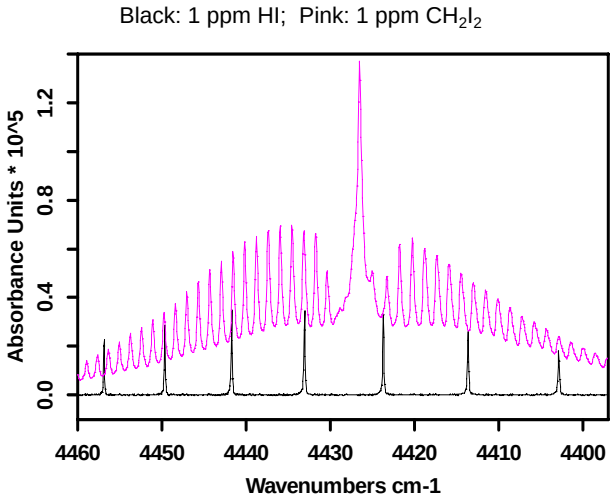

Fig. 4. Comparison plot (all at 0.1 cm^{-1} resolution) showing potential laser combination measurements using the CH_2I_2 ($\nu_2+\nu_6$) combination band at 4426.52 cm^{-1}. The traces correspond to 1 ppm-m of CH_2I_2 (upper trace – pink), and 1 ppm-m of hydrogen iodide, HI (lower trace – black). The spectra have been vertically offset for clarity.

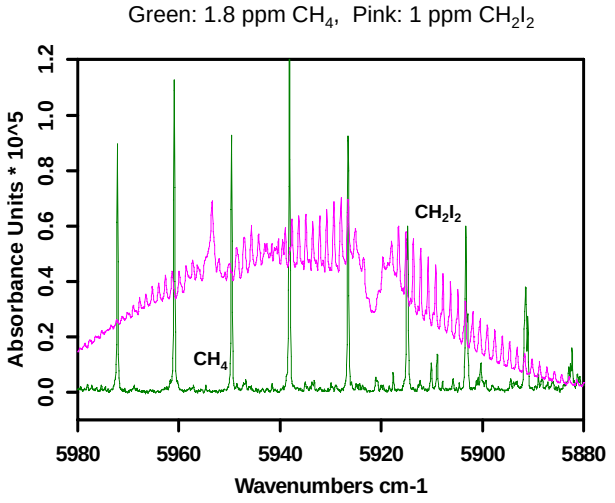

Fig. 5. Comparison plot (0.1 cm^{-1} resolution) showing potential laser combination measurements using the CH_2I_2 $2\,\nu_1$ overtone band (5921 cm^{-1}) along with the $\nu_1+\nu_6$ combination band at 5953 cm^{-1} along with the potential interference from CH_4. The traces correspond to 1 ppm-m of CH_2I_2 (upper trace – pink), and 1.8 ppm-m of methane, CH_4 (lower trace – green). The spectra have been vertically offset for clarity. See text for details.

Figure 4 plots the ($\nu_2+\nu_6$) combination band at 4426.52 cm^{-1} which we report for the first time. Figure 4's bottom trace also shows some of the sharp lines of the $2\nu_1$ overtone band of hydrogen iodide gas, HI. It was hoped that using a single laser it may be possible to simultaneously monitor both HI and CH_2I_2 by slight tuning of the wavelength. However, closer inspection of the database immediately showed that expected concentrations of 1.8 ppm_v of CH_4 or 316 ppbv of nitrous oxide (Evans and Puckrin, 1997) would interfere with such a measurement, particularly the N_2O. However, extractive measurements may still afford a practical separation of the HI/CH_2I_2 pair from the interfering signals, particularly at wavenumbers >4440 cm^{-1}, although wall adhesion mechanisms are of concern for species such as HI, HCl, or HNO_3 (Chackerian et al., 2003; Johnson et al., 2003). Nevertheless, such bands could be of use in e.g. a chamber kinetics study without CH_4 or N_2O.

The traces in Fig. 5 display two new bands of CH_2I_2, namely the $2\nu_1$ overtone (A_1 symmetry, B-type) at 5921.62 cm^{-1}, as well as the ($\nu_1+\nu_6$) combination C-type band at 5953.31 cm^{-1}. Both have resolved rotational structure even when pressure broadened to one atmosphere. The structure in these bands suggests the possibility of remote sensing as the Q-branch at 5953 cm^{-1} as well as several of the individual rotational lines, e.g. in the $2\nu_1$ R branch near 5930 cm^{-1} have differential absorbances of $\sim 3\times10^{-6}$. Such structure is very helpful not only for laser monitoring, but also for DOAS methods, which have been used to monitor trace gases such as HONO at the (sub-) ppbv levels (Platt et al., 1980). Detection limits of 10^{-4} are achievable, and path lengths of >10 km are now common. In a much related work Alicke and co-workers (1999) have used such a set-up in the UV-visible with a 14.6 km path to measure IO at levels of <10 ppt_v. For the case of CH_2I_2, if one assumes a 15 km (e.g. estuary) path and a differential cross section of 3×10^{-6} ppm-m (equivalent to 2.8×10^{-21} cm^2/molecule base-e) in order to observe 100 ppt_v of CH_2I_2 it would be necessary to detect an absorbance of 4.5×10^{-6} at these wavelengths. This is certainly a challenging detection limit, but DOAS detection for methane has recently been reported at these wavelengths (Frankenberg et al., 2005).

Of the CH_2I_2 near-infrared bands discussed above, several fortuitously display resolved structure, even when broadened to 1 atmosphere. Although the telecommunications diode lasers are limited in wavelength selection, several recent technologies offer methods for sensitive trace gas detection using such lines. These include tunable optical parametric oscillators, difference frequency generation (Richter et al., 2002) and, recently, red-shifting the emission wavelength of near-IR lasers via high pressures (Adamiec et al., 2004). In terms of the CH_2I_2 photochemistry in the presence of ozone, it may be possible to monitor the CH_2I_2, HI and IO simultaneously in a chamber type experiment as suggested by Mäkelä et al. (2002). The ν_6 3073 cm^{-1} band may be useful in laboratory experiments where CH_4 and H_2O concentrations are reduced. Also, monitoring at 3 μm offers the advantage of less light scattering compared to visible or NIR regions.

5 Summary

The quantitative infrared and near-infrared vapor-phase spectra of diiodomethane, CH_2I_2, have been reported for the first time. Using FT-IR and FT-Raman spectroscopy as well as ab initio computational methods we have completed a vibrational assignment. The atmospherically broadened spectra exhibit C-type bands near 5953, 4426 and 3073 cm^{-1} all have resolved rotational structure, including Q-branches with widths of $\sim$1 cm^{-1}. While GC-MS currently offers better sensitivity for point monitoring, some of the quantitative bands discussed here could be potentially useful for (remote) monitoring of this important species. The ν_6 Q-branch at 3073 cm^{-1} shows promise for extractive monitoring by Pb-salt or QC diode laser systems and the band strengths suggest estimated CH_2I_2 mixing ratios are near (or close to) the detection limit of current technology's best systems. The two very strong b_2 A-type bands (appearing as B-type, ν_9 at 584.21 cm^{-1} and ν_8 at 1113.87 cm^{-1}) do not resolve at atmospheric pressure, but show great promise for low pressure extractive laser studies. However, high resolution studies will first be needed.

The $\nu_1+\nu_6$ band shows a resolved Q-branch at 4426 cm^{-1}. While this band would be of little use for field measurements due to N_2O interferences, it could be used e.g. in smog chambers (synthetic air) with FTIR/laser spectrometers. As Fig. 4 depicts, it has the added benefit of being able to simultaneously measure the adjacent HI lines in a kinetics study. The two bands shown in Fig. 5 with strong structure near 5950 cm^{-1} may be of interest to e.g. the satellite-based DOAS systems as the long optical paths increase the burden for greater optical depth, and the wavelengths are just accessible on the red end of many current spectrometers.

Acknowledgements. We thank the referees for suggestions, particularly regarding the atmospheric chemistry. PNNL is operated for the U.S. Department of Energy by the Battelle Memorial Institute under contract DE-AC06-76RLO 1830. This work was supported under the DOE NA-22 program and we gratefully acknowledge that support. The experiment and calculations were performed at the W. R. Wiley Environmental Molecular Sciences Laboratory, a national scientific user facility sponsored by DOE's Office of Biological and Environmental Research and located at Pacific Northwest National Laboratory.

Edited by: J. N. Crowley

References

Adamiec, P., Salhi, A., Bohdan, R., Bercha, A., Dybala, F., Trzeciakowski, W., Rouillard Y., and Joullié, A.: Pressure-tuned InGaAsSb/AlGaAsSb Diode Laser with 700 nm Tuning Range, Appl. Phys. Lett., 85(19), 4292–4294, 2004.

Alicke, B., Hebestreit, K., Stutz J., and Platt, U.: Iodine Oxide in the Marine Boundary Layer, Nature, 397, 572–573, 1999.

Allen, G., Remedios, J. J., Newnham, D. A., Smith, K. M., and Monks, P. S.: Improved Mid-Infrared Cross-Sections for Peroxyacetyl nitrate (PAN) Vapour, Atmos. Chem. Phys., 5, 47–56, 2005, http://www.atmos-chem-phys.net/5/47/2005/.

Ballard, J., Strong, K., Remedios, J. J., Page, M., and Johnston, W. B.: A Coolable Long Path Absorption Cell for Laboratory Spectroscopic Study of Gases, J. Quant. Spec. Rad. Trans., 52, 677–691, 1994.

Bertie, J. E.: Specification of Components, Methods and Parameters in Fourier Transform Spectroscopy by Michelson and Related Interferometers, Pure Appl. Chem., 70(10), 2039, 1998.

Birk, M., Hausamann, D., Wagner G., and Johns, J. W.: Determination of Line Strengths by Fourier-transform Spectroscopy, Appl. Opt., 35, 2971–2985, 1996.

Bitter, M., Ball, S. M., Povey, I. M., and Jones, R. L.: A Broadband Cavity Ringdown Spectrometer for in situ Measurement of Atmospheric Trace Gases, Atmos. Chem. Phys., 5, 2547–2560, 2005, http://www.atmos-chem-phys.net/5/2547/2005/.

Bloss, W. J., Rowley, D. M., Cox, R. A., and Jones, R. L.: Kinetics and Products of the IO Self-reaction, J. Phys. Chem. A., 105, 7840–7854, 2001.

Burkholder, J. B., Curtius, J., Ravishankara A. R., and Lovejoy, E. R.: Laboratory Studies of the Homogeneous Nucleation of Iodine Oxide, Atmos. Chem. Phys., 4, 19–34, 2004, http://www.atmos-chem-phys.net/4/19/2004/.

Carpenter, L. J., Sturges, W. T., Penkett, S. A., Liss, P. S., Alicke, B., Hebestreit, K., and Platt, U.: Short-lived Alkyl Iodides and Bromides at Mace Head, Ireland: Links to Biogenic Sources and Halogen Oxide Production, J. Geophys. Res., 104(D1), 1679–1689, 1999.

Chackerian, C., Sharpe, S. W., and Blake, T. A.: Anhydrous Nitric Acid Integrated Cross Sections: 820–5300 cm^{-1}, J. Quant. Spectr. Rad. Transf., 82(1–4), 429–441, 2003.

Chameides, W. L. and Davis, D. D.: Iodine: Its Possible Role in Tropospheric Photochemistry, J. Geophys. Res., C, 85, 7383–7398, 1980.

Chase, D. B.: Nonlinear Detector Response and FT-IR, Appl. Spec., 38(4), 491–494, 1984.

Chu, P. M., Guenther, F. R., Rhoderick, G. C., and Lafferty, W. J.: The NIST Quantitative Infrared Database, J. Res. Natl. Inst. Stand. Technol., 104, 59, 1999.

Cox, R. A., Bloss, W. J., Jones, R. L., and Rowley, D. M.: OIO and the Atmospheric Cycle of Iodine, Geophys. Res. Lett., 26(13), 1857–1860, 1999.

Evans, W. F. J. and Puckrin, E.: A Wintertime Measurement of the Greenhouse Radiation from Nitrous Oxide, Can. J. Atmos. Sciences and Spectr., 42(5), 141–145, 1997.

Ford, T. A.: Infrared and Raman Spectra and Vibrational Assignments of Diiodomethane and Its Deuterated Analogs, J. Mol. Spec., 58, 185–193, 1975.

Frankenberg, C., Meirink, J. F., van Weele, M., Platt, U., and Wagner, T.: Assessing Methane Emissions from Global Space-Borne Observations, Science, 308, 1010–1014, 2005.

Gilles, M. K., Turnipseed, A. A., Burkholder, J. B., Ravishankara, A. R., and Solomon, S.: Kinetics of the IO radical: 2. Reaction of IO with BrO, J. Phys. Chem. A, 101, 5526–5534, 1997.

Griffith, D. W. T. and Jamie, I. M.: Fourier Transform Infrared

Spectrometry in Atmospheric and Trace Gas Analysis, in: Encyclopedia of Analytical Chemistry, edited by: Meyers, R. A., 1979–2000, 2000.

Harwood, M. H., Burkholder, J. B., Hunter, M., Fox, R. W., and Ravishankara, A. R.: Absorption Cross Sections and Self-reaction Kinetics of the IO radical, J. Phys. Chem. A, 101, 853–863, 1997.

Henry, B. R. and Hung, I.-F.: Mass Effects on the Applicability of local Mode Description of the High Energy Overtone Spectra of Difluoro-, Dichloro-, Dibromo- and Diiodomethane, Chem. Phys., 29, 465–475, 1978.

Himmelmann, S., Orphal, J., Bovensmann, H., Richter, A., Ladstätter-Weissenmayer, A., and Burrows, J. P.: First Observation of the OIO Molecule by Time-resolved Flash Photolysis Absorption Spectroscopy, Chem. Phys. Lett., 251, 330–334, 1996.

Hoffmann, T., O'Dowd, C. D., and Seinfeld, J. H.: Iodine oxide homogeneous Nucleation: An Explanation for Coastal New Particle Production, Geophys. Res. Lett., 28(10), 1949–1952, 2001.

Jimenez, J. L., Bahreini, R., Cocker III, D. R., Zhuang, H., Varutbangkul, V., Flagan, R. C., Seinfeld, J. H., O'Dowd, C. D., and Hoffman, T.: New Particle Formation from Photooxidation of Diiodomethane, J. Geophys. Res. D, 108(D10), 4318–4343, 2003.

Johnson, T. J., Roberts, B. A., and Kelly, J. F.: Semiactive Infrared Remote Sensing: A Practical Prototype and Field Comparison, Appl. Opt., 43(3), 638–650, 2004.

Johnson, T. J., Wienhold, F. G., Burrows, J. P., and Harris, G. W.: Frequency Modulation Spectroscopy at 1.3 μm Using InGaAsP Lasers: A Prototype Field Instrument for Atmospheric Chemistry Research, Appl. Opt., 30, 407–413, 1991a.

Johnson, T. J., Wienhold, F. G., Burrows, J. P., Harris, G. W., and Burkhard, H.: Measurements of Line Strengths in the HO_2 ν_1 Overtone Band at 1.5 μm Using an InGaAsP Laser, J. Phys. Chem., 95, 6499–6502, 1991b.

Johnson, T. J., Valentine, N. B., and Sharpe, S. W.: Mid-infrared versus Far-infrared (THz) Relative Intensities of Room-temperature *Bacillus* spores, Chem. Phys. Lett., 403, 152–157, 2005.

Johnson, T. J., Sams, R. L., Blake, T. A., Sharpe, S. W., and Chu, P. M.: Removing Aperture-Induced Artifacts from FTIR Intensity Values, Appl. Opt., 41, 2831–2839, 2002.

Johnson, T. J., Disselkamp, R. S., Su, Y.-F., Fellows, R. J., Alexander, M. L. and Driver, C. L.: Gas-phase Hydrolysis of $SOCl_2$: Implications for Its Atmospheric Fate, J. Phys. Chem. A, 107, 6183–6190, 2003.

Kasper, J. V. V., Parker, J. H., and Pimentel, G. C.: Atomic Iodine Photodissociation Laser, Appl. Phys. Lett., 5(11), 231–233, 1964.

Kasper, J. V. V., Parker J. H., and Pimentel, G. C.: Iodine-Atom Laser Emission in Alkyl Iodine Photolysis, J. Chem. Phys., 43, 1827–1828, 1965.

Kendall, R. A., Apra, E., Bernholdt, D. E., Bylaska, E. J., Dupuis, M., Fann, G. I., Harrison, R. J., Ju, J., Nichols, J. A., Nieplocha, J., Straatsma, T. P., Windus, T. L., and Wong, A. T.: High Performance Computational Chemistry: An Overview of NWChem, a Distributed Parallel Application, Computer Phys. Comm., 128, 260–283, 2000.

Kolb, C. E.: Iodine's Air of Importance, Nature, 417, 597–598, 2002.

Kroger, P. M., Demou, P. C., and Riley, S. J.: Polyhalide Photofragment Spectra. I. Two-photon Two-step Photodissociation of Methylene Iodide, J. Chem. Phys., 65(5), 1823–1834, 1976.

Mäkelä, J. M., Hoffmann, T., Holzke, C., Väkevä, M., Suni, T., Mattila, T., Aalto, P. P., Tapper, U., Kauppinen, E. I., and O'Dowd, C. D.: Biogenic Iodine Emissions and Identification of End-products in Coastal Ultrafine Particles during Nucleation Bursts, J. Geophys. Res., 107(D19), 8110–8124, 2002.

Maki, A., Blake, T. A., Sams, R. L., Vulpanovici, N., Barber, J., Chrysostom, E. T. H., Masiello, T., Nibler, J. W., and Weber, A.: High Resolution Infrared Spectra of the ν_2, ν_3, ν_4, and $2\nu_3$ bands of $^{32}S^{16}O_3$, J. Mol. Spectrosc., 210, 240–249, 2001.

Maki, A. G. and Wells, J. S.: Wavenumber Calibration Tables from Heterodyne Frequency Measurements, NIST Special Publication 821, National Institute of Standards and Technology, U.S. Government Printing Office, Washington, D.C., 1991.

Marshall, P., Srinivas, G. N., and Schwartz, M.: A Computational Study of the Thermochemistry of Bromine- and Iodine-Containing Methanes and Methyl Radicals, J. Phys. Chem. A, 109, 6371, 2005.

Masiello, T., Maki, A., and Blake, T. A.: The High-resolution Infrared Spectrum of $^{11}BF_3$ from 400 to 1650 cm^{-1}, J. Mol. Spectrosc., 234, 122–136, 2005.

McFiggans, G., Coe, H., Burgess, R., Allen, J., Cubison, M., Alfarra, M. R., Saunders, R., Saiz-Lopez, A., Plane, J. M. C., Wevill, D. J., Carpenter, L. J., Rickard, A. R., and Monks, P. S.: Direct Evidence for Coastal Iodine Particles from Laminaria Macroalgae – Linkage to Emissions of Molecular Iodine, Atmos. Chem. Phys. 4, 701–713, 2004.

Mertz, L.: Auxiliary Computation for Fourier Spectrometry, Infr. Phys., 7, 17, 1967.

Orphal, J. and Ibrahim, N.: The ν_1 and ν_6 Bands of Diiodomethane, CH_2I_2, around 3.3. Microns Studied by High-Resolution Fourier-Transform Spectroscopy, in: 19th Colloquium on High Resolution Molecular Spectroscopy, Salamanca, Spain, 11–16 September 2005.

Platt, U.: Differential Optical Absorption Spectroscopy, in: Monitoring by Spectroscopic Techniques, edited by: Sigrist, M. W., chapter 2, 27–84, Wiley & Sons, New York, 1994.

Platt, U., Perner, D., Harris, G. W., Winer, A. M., and Pitts, J. N.: Observations of Nitrous Acid in an Urban Atmosphere by Differential Optical-Absorption, Nature, 285, 312–314, 1980.

Richter, D., Fried, A., Wert, B. P., Walega, J. G., and Tittel, F. K.: Development of a Tunable mid-IR Difference Frequency Laser Source for Highly Sensitive Airborne Trace Gas Detection, Appl. Phys. B, 75, 281–288, 2002.

Rothman, L. S., Jacquemart, D., Barbe, A., Brenner, D. C., et al.: The HITRAN 2004 Molecular Spectroscopic Database, J. Quant. Spectrosc. Rad. Transf., 96, 139–204, 2005.

Rowley, D. M., Bloss, W. J., Cox, R. A., and Jones, R. L.: Kinetics and Products of the IO+BrO Reaction, J. Phys. Chem. A, 105, 7855–7864, 2001.

Schiller, C. L., Locquiao, S., Johnson, T. J., and Harris, G. W.: Atmospheric Measurements of HONO by Tunable Diode Laser Absorption Spectroscopy, J. Atmos. Chem., 40, 275–293, 2001.

Schmitt, G. and Comes, F. J.: Spectroscopic Investigations of the Photolysis of Diiodomethane, J. Mol. Struct., 61, 51–54, 1980.

Sharpe, S. W., Kelly, J. F., Hartman, J. S., Gmachl, C., Capasso, F., Sivco, D. L., Baillargeon, J. N., and Cho, A. Y.: High-

resolution (Doppler-limited) Spectroscopy Using Quantum-cascade Distributed-feedback Lasers, Opt. Lett., 23(17), 1396–1398, 1998.

Sharpe, S. W., Johnson, T. J., Chu, P. M., Kleimeyer, J., and Rowland, B.: Quantitative Infrared Spectra of Vapor Phase Chemical Agents, SPIE Proceedings, 5058, 19–27, 2003.

Sharpe, S. W., Johnson, T. J., Sams, R. L., Chu, P. M., Rhoderick, G. C., and Johnson, P. A.: Gas-phase Databases for Quantitative Infrared Spectroscopy, Appl. Spectr., 58(12), 1452–1461, 2004.

Solomon, S., Garcia, R. R., and Ravishankara, A. R.: On the Role of Iodine in Ozone Depletion, J. Geophys. Res., 99(D10), 20 491–20 499, 1994.

Tucceri, M. E., Hölscher, D., Rodriguez, A., Dillon, T. J., and Crowley, J. N.: Absorption cross section and photolysis of OIO, Phys. Chem. Chem. Phys., 8, 834–846, 2006.

Voelz, F. L., Cleveland, F., Meister, A. G., and Bernstein, R. B.: Substituted Methanes. XVII: Vibrational Spectra, Potential Constants, and Calculated Thermodynamic Properties of Diiodomethane, J. Opt. Soc. Am., 43, 1061–1064, 1953.

Vogt, R., Sander, R., von Glasow, R., and Crutzen, P. J.: Iodine Chemistry and Its Role in Halogen Activation and Ozone Loss in the Marine Boundary Layer, J. Atmos. Chem., 32, 375–395, 1999.

Volkamer, R., Molina, L. T., Molina, M. J., Shirley, T., and Brune, W. H.: DOAS Measurement of Glyoxal as an Indicator for Fast VOC Chemistry in Urban Air, Geophys. Res. Lett., 32, L08806, doi:10.1029/2005GL022616, 2005.

Warneck, P.: Chemistry of the Natural Atmosphere, p. 146 ff. Academic Press, San Diego, 1988.

Werle, P. W., Mazzinghi, P., D'Amato, F., De Rosa, M., Maurer, K., and Slemr, F.: Signal Processing and Calibration Procedures for in situ Diode-laser Absorption Spectroscopy, Spectrochimica Acta A, 60, 1685–1705, 2004.

Wert, B. P., Fried, A., Rauenbuehler, S., Walega, J., and Henry, B.: Design and Performance of a Tunable Diode Laser Absorption Spectrometer for Airborne Formaldehyde Measurements, J. Geophys. Res., 108(D12), 4350–4362, 2003.

Wevill, D. J. and Carpenter, L. J.: Automated Measurement and Calibration of Reactive Volatile Halogenated Organic Compounds in the Atmosphere, Analyst, 129, 634–638, 2004.

Williams, S. D., Johnson, T. J., Gibbons, T. P., and Kitchens, C. L.: Relative Raman Intensities in C_6H_6, C_6D_6, and C_6F_6: a Comparison of Different Computational Methods, Theo. Chem. Acc., in press, 2006.

Yaws, C. L.: Chemical Properties Handbook, McGraw-Hill, New York, 1999.